Mid-infrared spectroscopic thermotransmittance measurements in dielectric materials for thermal imaging

C. Bourges,[1,2] S. Chevalier,[1,2,*] J. Maire,[1,2,*] A. Sommier,[1,2] C. Pradere,[3] and S. Dilhaire[4]

1)Univ. Bordeaux, CNRS, Bordeaux INP, I2M, UMR 5295, F-33400, Talence, France

2)ENSAM, CNRS, Bordeaux INP, I2M, UMR 5295, F-33400 Talence, France

3)EPSYL-ALCEN, F-33400 Talence, France

4)Université de Bordeaux, LOMA, CNRS UMR 5798, F-33400 Talence, France

* Corresponding authors: stephane.chevalier@u-bordeaux.fr, jeremie.maire@u-bordeaux.fr

Abstract

Thermal considerations affect the performances of most microsystems. Although surface techniques can give information on the thermal properties within the material or about buried heat sources and defects, mapping temperature and thermal properties in three-dimension (3D) is critical and has not been addressed yet. Infrared thermography, commonly used for opaque materials, is not adapted to semitransparent samples such as microfluidic chips or semiconductor materials in the infrared range. This work aims at answering these needs by using the variations of transmittance with temperature to obtain information on the temperature within the thickness of the sample. We use a tunable mid-infrared light source combined with an infrared camera to measure these variations of transmittance in a glass wafer. We couple this technique with a thermal model to extract the thermotransmittance coefficient – the coefficient of temperature variation of the transmittance. We then introduce a semi-empirical model based on Lorentz oscillators to estimate the temperature-dependent optical properties of our sample in the mid-IR spectral range. Combined with the measurements, this paper reports both

explanation and prediction of the spectroscopic behavior of the thermotransmittance coefficient in the mid-IR range

Main text

Although microsystems are increasingly subject to thermal challenges, there is no reliable contactless way to measure the temperature within a device for all types of materials. In most cases, surface measurements performed by detecting the reflection of a light beam [1–4] or the infrared (IR) [5–7] emission from the surface are coupled to thermal models and inverse methods to estimate the temperature in buried layers and thermal properties such as thermal diffusivity [8] or thermal contact resistance between layers [9]. However, these approaches are often developed for opaque surfaces and quantitative measurements in semi-transparent media proves more challenging. In these materials, the volume of the sample contributes to the proper emission measured in IR thermography and an apparent emissivity [10] or emittance [11] needs to be defined. Furthermore, the camera needs to be calibrated and background noise from the environment need to be filtered out [12]. Although IR thermography is therefore not yet widely used, several works have either focused on measuring the emittance [12–14] or on the thermal diffusivity of the material. Despite these studies, developments of contactless measurement of the 3D temperature field in semitransparent media remain necessary. This is especially true in the IR spectral range, particularly from 2 to 5 µm. With the strong development of microsystems semi-transparent in that spectral range, such as microfluidic chips, electronic devices, energy generation and storage devices like micro-batteries and supercapacitors, there is an increasing need for *operando* temperature measurement within these systems. In a previous work, we have demonstrated the possibility to overcome the challenges inherent to semi-transparent media without the need for

emittance measurements by performing temperature measurements based on the thermotransmittance technique in the mid-IR range [15].

Thermotransmittance consists in illuminating the sample of interest with a light source and measuring the signal transmitted through that sample. When the sample is subjected to temperature variations, its optical properties vary locally where temperature changes. This will in turn be detected as a change in the transmitted signal that can be approximated as a first-order function of the temperature. There is therefore a proportionality coefficient between the temperature change and the corresponding transmittance variation, which we call the thermotransmittance coefficient $\kappa(\lambda)$, where λ stands for the wavelength. This change in the optical properties related to a change in temperature is often used in the visible or near-IR range in thermoreflectance or thermotransmittance [16,17] and preliminary studies have demonstrated thermotransmittance measurements in both the mid-IR [18] and terahertz [19] spectral ranges. Since the thermotransmittance signal can be affected by both surface reflectance variations and absorbance variations, its potential applications span many materials. Kakuta et al. [20,21] have investigated the temperature dependence of the absorption in water-ethanol mixtures in the near-IR and used the thermal dependence of the absorption to study convection phenomena [22,23] and temperature fields [24] in aqueous solutions. Yu et al. [25,26], on the other hand, have studied the absorption spectrum of fused silica fiber optics in the near infrared (1000 – 2500 nm) as a function of temperature, focusing on the hydroxyl groups. The relative lack of data concerning the thermotransmittance and the optical properties of materials in the mid-IR, however, illustrates the need for reliable measurements of the thermotransmittance coefficient, but also for a way to predict it. This is all the more problematic that the measurement of temperature relies on the a priori knowledge of this coefficient. To enable accurate predictions, the mechanisms behind the thermotransmittance coefficient should therefore be clarified.

The origin of the thermotransmittance coefficient, $\kappa(\lambda)$, lies in the variation of the optical properties with temperature, and in particular the reflections at interfaces and the absorption in the material. The Lorentz oscillators model describes the response of the bound electrons to an electric field and allows the calculation of the relative permittivity and therefore the refractive index, based on electrons collectively acting as damped oscillators. The resulting temperature dependence of the refractive index then translates to a temperature dependence of the reflection and transmission. It can therefore appropriately model dielectric materials' properties in the mid-IR range to obtain the wavelength dependent thermotransmittance coefficient. In our previous work, the wavelength was selected without consideration for the wavelength dependence of the thermotransmittance coefficient [15], which strongly limits the performance of this technique. However, another study focusing on a microfluidic chip highlighted the importance of the choice of wavelength for the simultaneous imaging of temperature and concentration [21]. Thus, it clearly appears that a phenomenological model to predict the thermotransmittance coefficient, and its extensive measurement in the mid-IR range would be of fundamental importance to strengthen the temperature measurements in semi-transparent dielectric materials.

Therefore, this work aims at answering these needs by reporting the measurements of κ as a function of wavelength in the mid IR range, and by proposing a Lorentz oscillators model with thermodependent parameters to predict the value of κ as a function of wavelength. The experimental setup relies on an IR camera to detect the variations of transmission from an IR source through a Borofloat glass wafer heated at different temperatures [15]. We then introduce a semi-empirical expression of the transmittance based on Lorentz oscillators and compare the results to the transmission spectrum at ambient temperature. Finally, we introduce the temperature dependence in the model and fit the free parameters to the thermotransmittance coefficients measured at different wavelengths to obtain the thermotransmittance coefficient

spectrum between 3100 nm and 4600 nm and provide measurements to justify the choice of measurement wavelength.

The measurement process consists in using IR camera to detect the intensity of an IR beam that is transmitted through the sample of interest. As the temperature of the sample changes, so do the optical properties of the sample and the corresponding variation in the intensity of the transmitted beam is recorded; it can be expressed as follows:

$$\frac{\Delta\Gamma(t,\lambda)}{\Gamma_0(\lambda)} = \kappa(\lambda)\Delta T(t), \qquad \text{Eq. 1}$$

where $\Gamma_0(\lambda)$ is the transmittance at ambient temperature T_0, $\Delta\Gamma(t,\lambda) = \Gamma(T,t,\lambda) - \Gamma_0(\lambda)$ is the variation in the transmitted signal as a function of temperature at time t, $\Delta T(t) = T(t) - T_0$ is the variation of temperature as a function of the same time t. Note that since the optical properties depend on the wavelength λ, so does the thermotransmittance coefficient and therefore the measured relative transmittance variation.

To measure the thermotransmittance signal, we use the setup shown in Figure 1. The illumination wavelength is selected using a diffraction grating monochromator (Bentham Instruments, TMc300) from a stabilized broadband infrared lamp (IR-Si217), before passing through a beam expander to adjust the diameter of the IR beam to match the sample dimensions. The transmitted IR beam is then detected using an infrared camera (FLIR SC7000), equipped with an indium-antimonide (InSb) detector of 512×640 pixels, a pixel pitch of 15 µm, and a 50 mm focal length lens. The spectral range of the camera is $\lambda \in [2.5 - 5.5]$ µm, and the optical resolution is 107 µm/pixel in our experimental configuration.

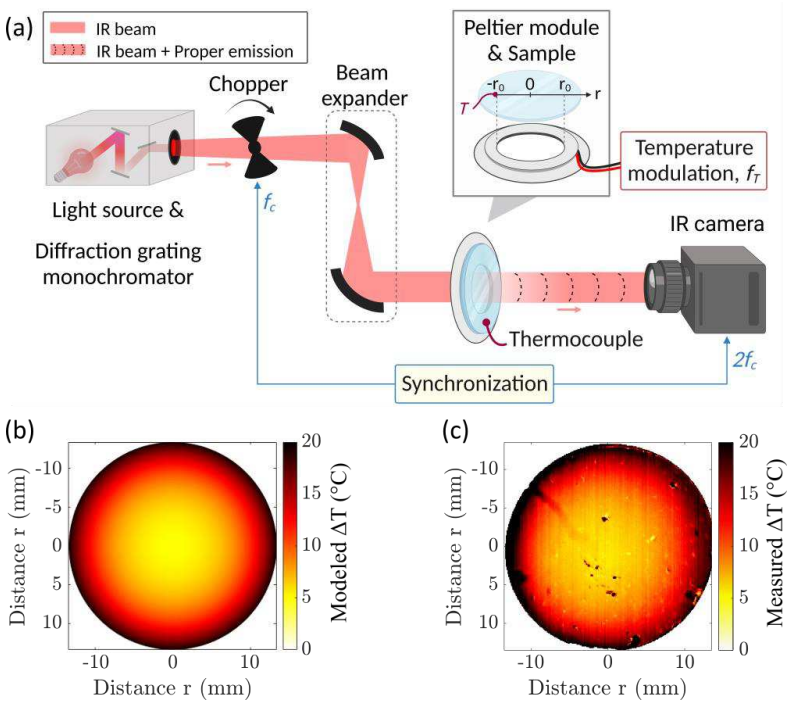

Figure 1. a) Thermotransmittance measurement system. The light source, comprising an IR lamp and a monochromator, shines through a beam expander and through the sample, and is detected by an IR camera. The camera acquisition is synchronized to an optical chopper to alternatively acquire images with and without the IR beam. **insert:** The glass sample mounted on the annular Peltier module. **b, c)** Amplitude field of the modeled and measured temperatures.

The signal S measured by the camera is the sum of the proper emission E of the scene and the IR beam transmitted by the sample I, i.e., $S = E + I$. As we are only interested in variations of I, the source chopping method is employed to separate these contributions: the chopper opening provides S, while its closing provides only the radiations from the scene E. The camera acquisition frame rate is synchronized at twice the chopper frequency $2f_c$. To retrieve I, two successive frames are subtracted, assuming no variation in the proper emission intensity

between these two frames, and the process is repeated every two frames. This hypothesis is valid only if the chopper frequency f_c is very large in front of the thermal variations' frequency f_T. Therefore, we set f_c much larger than f_T, with $f_c = 25$ Hz and $f_T = 5$ mHz.

To demonstrate this method, we use a wafer of Borofloat® 33 glass, which is a semitransparent insulator within the camera's spectral range. The sample has a diameter of $d = 50.8$ mm and a thickness of $L = 515 \pm 10$ µm. To measure the variations of the transmitted intensity as a function of temperature, we use an annular Peltier module to modulate the temperature of the sample around T_0 at the frequency f_T: $T(t,r) = T_0 + \Delta T(r)\cos(2\pi f_T t)$, with r the distance from the center of the sample. The thermal connection between the sample edges ($r > r_0$) and the inner edge of the Peltier module is ensured by thermal paste. A separate temperature monitoring of the sample is achieved via a thermocouple combined with a custom-made LabView software. The amplitude variation of the temperature is set to 20 K at the inner edge of the Peltier module ($r = r_0$). The corresponding calculated temperature map is shown in Fig. 1b for a thermal diffusivity fixed at the measured value of $a = 8.2 \pm 0.7 \times 10^{-7}$ m^2/s [27,28]. The procedure to obtain the thermal properties of the sample is detailed in our previous work [15]. The measured temperature variation field $\Delta T(r)$ after demodulating the thermotransmittance signal at frequency f_T is shown in Fig. 1c.

The first step in comprehending the temperature dependency of transmission though a semitransparent sample consists in modeling the optical properties and calibrating the setup. The optical behavior of the materials can then be predicted and the most thermally sensitive wavelengths can be identified to optimize experimental studies.

To determine the total transmittance of a slide of thickness L, we need to consider (i) the reflections at the sample interfaces, (ii) the absorption in the material and (iii) the contribution

of multiple reflections that occur within the slide [29]. The total transmission coefficient, Γ_{tot}, is obtained by summing the contributions from multiple reflections as given in Equation 2:

$$\Gamma_{tot}(\lambda) = (1 - R(\lambda))^2 \times e^{-\alpha(\lambda)L} \times \sum_{q=1}^{\infty} R(\lambda)^{2(q-1)}\, e^{-2(q-1)\alpha(\lambda)L}, \qquad \textit{Eq. 2}$$

where the reflection coefficient R and the absorption α are given by the following equations:

$$R(\omega) = \frac{(n'(\omega) - 1)^2 + n''^2(\omega)}{(n'(\omega) + 1)^2 + n''^2(\omega)}, \qquad \textit{Eq. 3}$$

$$\alpha(\omega) = \frac{2\omega n''(\omega)}{c} = \frac{4\pi n''(\omega)}{\lambda}, \qquad \textit{Eq. 4}$$

where n' and n'' stand for the real and imaginary part of the refractive index $\tilde{n}(\omega) = n'(\omega) + in''(\omega)$ and where the angular frequency is given by $\omega = 2\pi c/\lambda$, and c is the speed of light in vacuum (m/s).

Both parts can be calculated from the relative permittivity $\tilde{\varepsilon}_r(\omega) = \varepsilon'(\omega) + i\varepsilon''(\omega)$ with the following set of equations:

$$n'(\omega) = \sqrt{\frac{\sqrt{\varepsilon'^2(\omega) + \varepsilon''^2(\omega)} + \varepsilon'(\omega)}{2}}, \qquad \textit{Eq. 5}$$

$$n''(\omega) = \sqrt{\frac{\sqrt{\varepsilon'^2(\omega) + \varepsilon''^2(\omega)} - \varepsilon'(\omega)}{2}}. \qquad \textit{Eq. 6}$$

In our modeling approach, we assume that the dielectric properties of the transparent medium are well-described by a classical Lorentz oscillators' behavior that is characterized by the total permittivity. This complex value is the sum the dielectric constant ε_∞ and the contributions of

several resonances processes, which can be modeled as a sum of oscillators. Each oscillator is then characterized by its resonance and plasma frequencies ω_O and ω_p, as well as a damping factor γ. The resulting expression for the permittivity is given in Equation 7:

$$\widetilde{\varepsilon_r}(\omega) = \varepsilon_\infty + \sum_j \frac{\omega_{p,j}^2}{\omega_{0,j}^2 - \omega^2 + i\omega\gamma_j} \qquad \textit{Eq. 7}$$

These parameters are not known a priori, and transmission measurements are required to set them. We use the setup shown in Fig. 1 at ambient temperature and sweep the wavelength of the monochromator over the detection range of our camera. The resulting transmission and reflection spectra are shown in Fig. 2. Several features are visible, such as three dips of varying depth in the transmission and a progressive decrease of the transmission at large wavelengths. Therefore, we choose the resonant frequencies of the oscillators so that they correspond to the three dips as well as one chosen arbitrarily at a wavelength beyond 5000 nm to model the progressive decrease in transmission. The chosen values are reported in Table 1 and are in good agreement with the literature [30,31]. Although our values agree, note that the bound electrons resonances do not necessarily explain the physical or chemical origin of these bands, which have been explained at length in previous works, such as OH groups in oxide glasses [32] or B2O3 and Na2O/K2O dopants [33].

Wavelength (nm)	2750	3620	3960	5500
Resonant frequency ω_0 (rad/s)	6.85×10^{14}	5.20×10^{14}	4.76×10^{14}	3.43×10^{14}

Table 1. Identified resonant frequencies

Next, we perform an optimization to estimate all the remaining unknowns, namely the plasma frequencies, the damping rates and the dielectric constant. The latter was found to be $\varepsilon_\infty =$

2.6 ± 0.3, again in agreement with the literature [31], and the remaining parameter values are given in Table 2. The details of the optimization and sensitivities to the different parameters are given in Supplementary Materials.

Wavelength λ (nm)	Plasma pulsation ω_p (rad/s)	Damping rate γ (s^{-1})
2750	$3.1 \pm 0.3 \times 10^{12}$	$3.3 \pm 0.8 \times 10^{13}$
3620	$4.8 \pm 0.2 \times 10^{12}$	$2.5 \pm 0.3 \times 10^{13}$
3960	$4.2 \pm 0.5 \times 10^{12}$	$3.8 \pm 0.8 \times 10^{13}$
5500	$1.4 \pm 0.4 \times 10^{13}$	$1.2 \pm 0.6 \times 10^{12}$

Table 2. Best fit values of the plasma frequencies and the damping rates.

The result of the fit is shown in Fig. 2 alongside the measured spectrum. The approach of assimilating spring-bound electrons in the Lorentz oscillators model with several resonance frequencies gives results in good agreement with the experimental values, as the position, width and depth of the dips in transmission are well reproduced. However, the discrepancy observed between the measurement and the model for the transmission peak around 3300 nm suggests that other types of contributions are missing from the model such as that of free electrons [34], or contributions that could be accounted for by a semi-quantic dielectric function model [35]. Another possibility is that the visible and near infrared absorption peaks are not considered in the model, which could have a slight impact on the peak at 3300 nm. Several more complex models have been proposed [36–39] that account for various phenomena, and some of the spectral features were attributed to the fabrication process. More complex models have been developed in the literature to account for all the phenomena Nonetheless, despite the highly non-monotonous transmission spectrum of our sample, the absolute error, calculated as the difference between the measured and modeled value, remains below 10%. The best fit therefore

provides a basis for introducing the temperature dependence in the coefficients of the semi-empirical model.

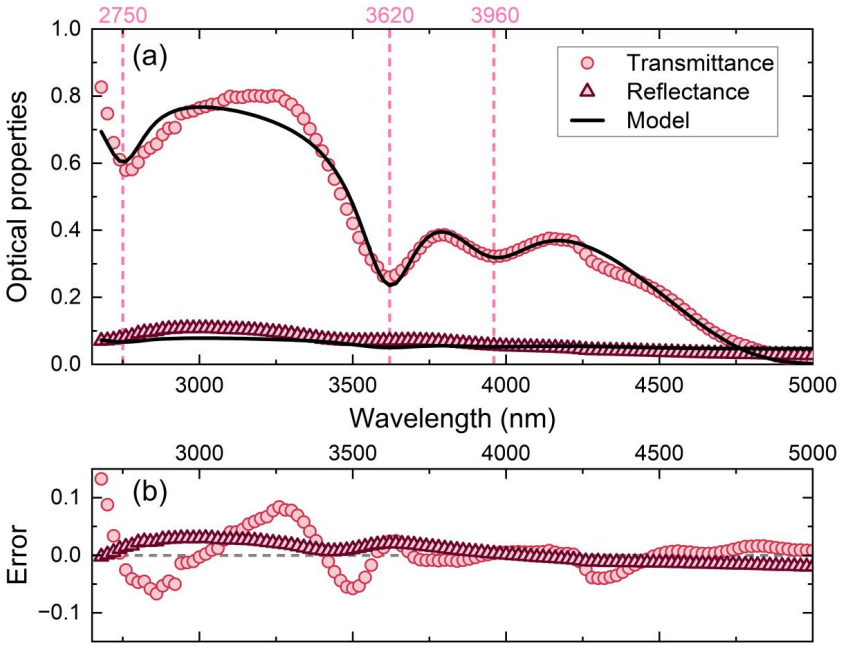

Figure 2. Transmittance and reflectance spectra. a) Spectral transmittance and reflectance of the Borofloat wafer measured experimentally (solid lines) and modeled (dashed lines). The three resonances corresponding to the dips in transmittance are indicated with the dashed lines. **b)** Absolute error for both the transmittance and reflectance spectra.

Once we have identified all the parameters at ambient temperature, we investigate the thermal dependency of the refractive index and its impact on the transmittance of the material. For simplicity, we assume that the resonant frequencies, plasma frequencies and damping rates are first-order functions of temperature given by Eq. 8-10.

$$\omega_0(T) = \omega_0(T_0) \times \left(1 + \alpha_{\omega_0} \Delta T\right) \qquad \textit{Eq. 8}$$

$$\omega_p(T) = \omega_p(T_0) \times \left(1 + \alpha_{\omega_p} \Delta T\right) \quad \textit{Eq. 9}$$

$$\gamma(T) = \gamma(T_0) \times \left(1 + \alpha_{\gamma} \Delta T\right) \quad \textit{Eq. 10}$$

where $\Delta T = T - T_0$ is the temperature variation (K) and α_{ω_0}, α_{ω_p} and α_{γ} the coefficients of thermal variation of the resonant frequencies, plasma frequencies and damping rates, respectively (K^{-1}). The values at $T = T_0$ correspond to the room-temperature values obtained in the previous section. For the plasma frequencies, the temperature dependence is primarily caused by the thermal expansion of the material that affects the electron density $n_e(T)$ [40].

To estimate the temperature coefficients for each resonance identified in the previous section, we need the experimental values of the thermotransmittance coefficient. We extract the thermotransmittance coefficient at each wavelength of interest using the method described in our previous work from the thermal fields shown in Fig. 1b,c. The variation of transmittance as a function of temperature is presented in Fig. 3a for the wavelength $\lambda = 3300$ nm and clearly shows a linear dependence. A linear regression then provides the thermotransmittance coefficient. Note that the higher dispersion in the thermotransmittance signal for large temperature variations correspond to pixels close to the contact area with the Peltier module used to modulate the temperature, where there is uncertainty about the exact position of the edge. We repeat the same procedure at selected wavelengths from 3100 nm to 4600 nm and plot the values of the thermotransmittance coefficient as a function of the wavelength.

The temperature-dependent model is then fitted to the thermotransmittance signal as a function of wavelength with a simplex minimization algorithm [41]. The resulting temperature coefficients are shown in Table 3. The modeled thermotransmittance as a function of wavelength is plotted in the range from 3000 nm to 5000 nm in Fig. 3b alongside the experimental values. The good agreement between the experimental values and the best fit from the model attests that our model is a good approximation to calculate the thermo-optical

properties of semitransparent materials, although different interactions should be considered to obtain more refined spectral features.

Wavelength λ (nm)	Coefficient α_{ω_0} (K^{-1})	Coefficient α_{ω_p} (K^{-1})	Coefficient α_{γ} (K^{-1})
2750	-4.5×10^{-5}	2.5×10^{-2}	2.8×10^{-2}
3620	-7.6×10^{-6}	2.0×10^{-5}	-5.5×10^{-5}
3960	-1.1×10^{-5}	5.6×10^{-4}	-8.5×10^{-4}
5500	-1.2×10^{-4}	4.7×10^{-4}	-9.1×10^{-4}

Table 3. Coefficient of temperature dependence for the three parameters for each of the resonance wavelength.

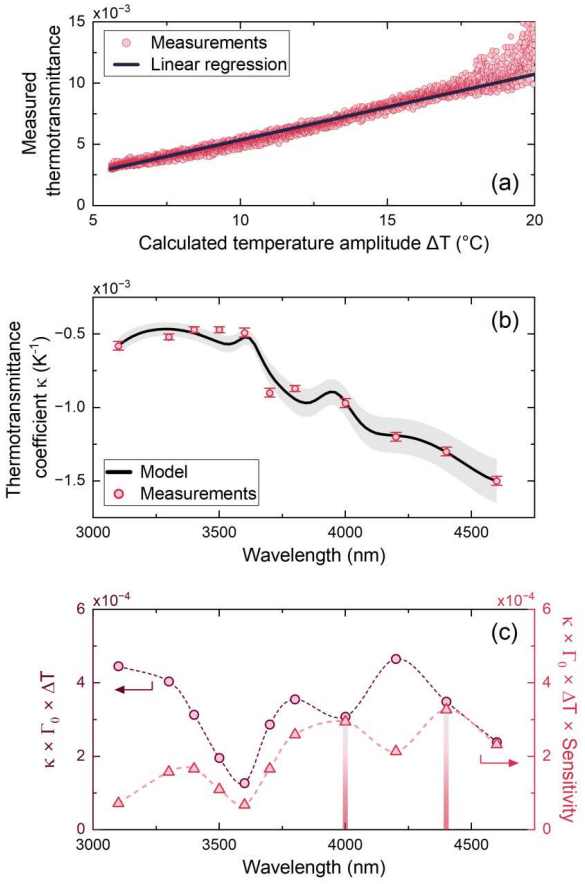

Figure 3. a) Relative variation of the transmittance as a function of the calculated temperature. **b)** Extracted thermotransmittance coefficient for different wavelengths and comparison to the temperature-dependent optical model output. **c)** Total transmitted signal arriving on the detector for a unitary temperature increase (circles, left) and corresponding signal weighed by the transfer function of the whole acquisition chain (triangles, right).

Since the intensity of the transmittance variation with temperature is represented by the absolute value of the thermotransmittance coefficient, we see from Fig. 3 that the relative variation of transmission as a function of temperature will increase for longer wavelengths in the range investigated in this study. More specifically, the thermotransmittance scales with the absorbance and an illumination wavelength matching an absorbance peak – equivalent to a transmittance dip – gives the highest value of the thermotransmittance coefficient. To elucidate the reason behind this, we first introduce a first order temperature dependence in the reflectance and in the absorption coefficient, similarly to what has been done for the optical parameters. After injecting these new expressions in Eq. 2, we calculate the temperature dependent relative variation of transmittance, that is our thermotransmittance signal. The resulting expression can then be linearized to obtain

$$\frac{\Delta\Gamma}{\Gamma_0} \approx \left(\frac{2R_0\kappa_r}{1-R_0} - \alpha\kappa_\alpha L\right)\Delta T, \qquad \textit{Eq. 11}$$

where Γ_0 is the initial transmittance at ambient temperature, $\Delta\Gamma$ is the variation of transmittance for a variation of temperature ΔT, κ_r and κ_α are phenomenon-specific thermotransmittance coefficients from the reflectance and absorbance, with κ_r expressed in K^{-1} and κ_α expressed in K^{-1}. We can see from this expression that by measuring samples with identical properties but different thicknesses, it will be possible to accurately measure the relative contributions of reflectance and absorbance to the measured signal, which will be investigated in a future work. Therefore, measurements will strongly vary based on the thickness of the sample. All the values of the thermotransmittance coefficient are given here in K^{-1}, and are thus valid for a given thickness of the material – the thickness dependence of this coefficient will be the subject of a further study.

These observations do not necessarily mean that longer wavelengths are more appropriate to perform thermotransmittance measurements, as the response of the whole acquisition chain has to be considered (see its spectral transfer function in Fig. S5 of the

supplementary material). The measured signal variation indeed combines the relative variation due to temperature changes, but also the absolute value of the transmitted signal. The product of these two values, shown in Fig. 3c, shows a large dispersion in our particular sample but, although several wavelengths, both short and long, display high values, no single one stands out as the best choice for measurements. The measured intensity variation also depends on the transfer function of the whole acquisition chain, among which the sensitivity of the detector. The total signal output by the camera as a function of wavelength, given in Fig. 3c, clearly highlights the best wavelengths to perform thermotransmittance measurements with our experimental setup, here around 4000 nm and 4400 nm for this particular sample. It is interesting to note the decrease in signal between the two curves of Fig. 3c around 4200 nm, which corresponds to the absorption peak of the CO_2 present in the air. One of the interests of these spectroscopic measurements therefore lies in finding the wavelength at which the signal to noise ratio will be optimal.

In conclusion, we developed a semi-empirical model to estimate the temperature-dependent optical properties of dielectric materials, such as glass, in the mid-IR spectral range. The model is combined with thermotransmittance measurements that consist in measuring the temperature-dependent transmission through the material, to obtain the transmission and reflection spectra, as well as the thermotransmittance coefficient. This approach completes our previous work in which we have demonstrated the ability of thermotransmittance measurements to extract the temperature fields and thermal diffusivity of semi-transparent materials in the mid-IR spectral range. This work sheds light on how the thermotransmittance signal varies with the source wavelength and acquisition chain sensitivity.

More specifically, we have introduced here a formalism based on Lorentz oscillators and shown that a fit to the experimental data could help us choose an ideal wavelength for

thermotransmittance measurements. Even in the restricted spectral range of study in this work, the thermotransmittance vary by as much as a factor three, showing that there are potentially wavelengths at which some materials are sensitive and others not. This discrepancy can allow to distinguish the origin of the thermotransmittance signal at specific wavelengths in heterogeneous structures. Derivating our model further can also help predict the dependence over other parameters, such as the sample thickness. With this thickness dependence, it becomes possible to quantitatively assess the proportion of the thermotransmittance signal stemming from reflectance and that coming from the absorbance of the material, which will be detailed in a future work. Overall, this work expands our previous demonstration of thermotransmittance to spectroscopic measurements that combine with a simple semi-empirical model to optimize temperature imaging in semi-transparent media.

Supplementary Material

The Supplementary Material presents a sensitivity analysis of the model and the fit parameters. Additional details concerning the sample thickness dependence of transmittance, the extraction of the thermotransmittance coefficient at different wavelengths and the spectral sensitivity of the measurement are also given. It is divided in five sections:

1. Relative contribution of each resonance position and parameters to the transmittance spectrum
2. Sensitivity analysis on the temperature coefficients
3. Impact of sample thickness on the transmission spectrum
4. Extraction of the thermotransmittance coefficient at different wavelengths
5. Transfer function of the acquisition chain

Acknowledgments and statements

This work was supported by the French National Research Agency (ANR) (Grant ANR-22-CE50-0015).

The authors declare no conflict of interest.

References

[1] P.M. Norris, A.P. Caffrey, R.J. Stevens, J.M. Klopf, J.T. McLeskey, A.N. Smith, *Femtosecond pump–probe nondestructive examination of materials (invited)*, Rev. Sci. Instrum. **74** (2003) 400–406.

[2] R. Anufriev, S. Gluchko, S. Volz, M. Nomura, *Quasi-Ballistic Heat Conduction due to Lévy Phonon Flights in Silicon Nanowires*, ACS Nano. **12** (2018) 11928–11935.

[3] K. Yazawa, D. Kendig, J. Christofferson, A. Marconnet, A. Shakouri, *Fast Transient and Steady State Thermal Imaging of CMOS Integrated Circuit Chips Considering Package Thermal Boundaries*, (n.d.).

[4] D.G. Cahill, K. Goodson, A. Majumdar, *Thermometry and Thermal Transport in Micro/Nanoscale Solid-State Devices and Structures*, J. Heat Transfer. **124** (2002) 223.

[5] F. Cernuschi, A. Russo, L. Lorenzoni, A. Figari, *In-plane thermal diffusivity evaluation by infrared thermography*, Rev. Sci. Instrum. **72** (2001) 3988–3995.

[6] M.M. Groz, A. Sommier, E. Abisset, S. Chevalier, J.L. Battaglia, J.C. Batsale, C. Pradere, *Thermal resistance field estimations from IR thermography using multiscale Bayesian inference*, Quant. Infrared Thermogr. J. **18** (2021) 332–343.

[7] O. Breitenstein, M. Langenkamp, F. Altmann, D. Katzer, A. Lindner, H. Eggers, *Microscopic lock-in thermography investigation of leakage sites in integrated circuits*, Rev. Sci. Instrum. **71** (2000) 4155–4160.

[8] A. Bedoya, J. González, J. Rodríguez-Aseguinolaza, A. Mendioroz, A. Sommier, J.C. Batsale, C. Pradere, A. Salazar, *Measurement of in-plane thermal diffusivity of solids moving at constant velocity using laser spot infrared thermography*, Measurement. **134** (2019) 519–526.

[9] C. Chassain, A. Kusiak, K. Krause, M. Garcia, J.-L. Battaglia, *Bayesian Estimation of Thermal Properties Using Periodically Pulsed Photothermal Radiometry: A Focus on Interfacial Thermal Resistances between Layers*, Phys. Status Solidi – Rapid Res. Lett. **17** (2023).

[10] J. Gieseler, A. Adibekyan, C. Monte, J. Hollandt, *Apparent emissivity measurement of semi-transparent materials part 2: Theoretical concept*, J. Quant. Spectrosc. Radiat. Transf. **258** (2021) 107317.

[11] S. Jeon, S.-N. Park, Y.S. Yoo, J. Hwang, C.-W. Park, G.W. Lee, *Simultaneous measurement of emittance, transmittance, and reflectance of semitransparent materials at elevated temperature*, Opt. Lett. **35** (2010) 4015.

[12] J. Gieseler, A. Adibekyan, C. Monte, J. Hollandt, *Apparent emissivity measurement of semi-transparent materials part 1: Experimental realization*, J. Quant. Spectrosc. Radiat. Transf. **257** (2020) 107316.

[13] O. Rozenbaum, D.D.S. Meneses, Y. Auger, S. Chermanne, P. Echegut, *A spectroscopic method to measure the spectral emissivity of semi-transparent materials up to high temperature*, Rev. Sci. Instrum. **70** (1999) 4020–4025.

[14] A. Adibekyan, E. Kononogova, C. Monte, J. Hollandt, *Review of PTB Measurements on Emissivity, Reflectivity and Transmissivity of Semitransparent Fiber-Reinforced Plastic Composites*, Int. J. Thermophys. **40** (2019) 36.

[15] C. Bourgès, S. Chevalier, J. Maire, A. Sommier, C. Pradère, S. Dilhaire, *Infrared thermotransmittance-based temperature field measurements in semitransparent media*, Rev. Sci. Instrum. **94** (2023) 034905.

[16] E.A.A. Pogna, X. Jia, A. Principi, A. Block, L. Banszerus, J. Zhang, et al., *Hot-Carrier Cooling in High-Quality Graphene Is Intrinsically Limited by Optical Phonons*, ACS Nano. **15** (2021) 11285–11295.

[17] H. Search, C. Journals, A. Contact, M. Iopscience, I.P. Address, *CCD-based thermoreflectance microscopy : principles and applications*, **143001** (n.d.).

[18] C. Pradere, M. Ryu, A. Sommier, M. Romano, A. Kusiak, J.L. Battaglia, J.C. Batsale, J. Morikawa, *Non-contact temperature field measurement of solids by infrared multispectral thermotransmittance*, J. Appl. Phys. **121** (2017) 085102.

[19] M. Bensalem, A. Sommier, J.C. Mindeguia, J.C. Batsale, L.-D. Patino-Lope, C. Pradere, *Contactless Transient THz Temperature Imaging by Thermo-transmittance Technique on Semi-transparent Materials*, J. Infrared, Millimeter, Terahertz Waves. **39** (2018) 1112–1126.

[20] N. Kakuta, Y. Fukuhara, K. Kondo, H. Arimoto, Y. Yamada, *Temperature imaging of water in a microchannel using thermal sensitivity of near-infrared absorption*, Lab Chip. **11** (2011) 3479.

[21] N. Kakuta, H. Yamashita, D. Kawashima, K. Kondo, H. Arimoto, Y. Yamada, *Simultaneous imaging of temperature and concentration of ethanol–water mixtures in microchannel using near-infrared dual-wavelength absorption technique*, Meas. Sci. Technol. **27** (2016) 115401.

[22] N. Kakuta, Y. Arakawa, M. Kyoda, T. Miyake, K. Mishiba, K. Kondo, *Near-infrared measurement of axisymmetric temperature field formed by free convection from a 1-mm-diameter heating sphere in water*, Int. J. Heat Mass Transf. **137** (2019) 847–856.

[23] T.-A. Nguyen, K. Kondo, N. Kakuta, *Near-infrared measurement of temperature fields formed by mixed convection from a small heating sphere in water*, Int. J. Therm. Sci. **176** (2022) 107498.

[24] V.-C. Han, N. Kakuta, *Near-infrared measurement of water temperature near micro-magnetic particle layer in a fluidic channel under induction heating*, Exp. Therm. Fluid Sci. **115** (2020) 110087.

[25] L. Yu, E. Bonnell, D. Homa, G. Pickrell, A. Wang, P.R. Ohodnicki, S. Woodruff, B. Chorpening, M. Buric, *Observation of temperature dependence of the IR hydroxyl absorption bands in silica optical fiber*, Opt. Fiber Technol. **30** (2016) 1–7.

[26] L. Yu, D. Homa, P. Ohodnicki, M. Buric, B. Chorpening, G. Pickrell, A. Wang, *Thermally induced emission from hydroxyl groups in fused silica optical fibers*, Opt. Fiber Technol. **52** (2019) 101951.

[27] E.G. Williamson, E. Lloyd-Jones, M.R. Smith, *A Compilation of thermal property data for computer heat-conduction calculations*, 1954.

[28] S.W. Churchill, H.H.S. Chu, *Correlating equations for laminar and turbulent free convection from a vertical plate*, Int. J. Heat Mass Transf. **18** (1975) 1323–1329.

[29] Eugene Hecht, *Optics: International Edition*, Pearson, 2003.

[30] K.M. Davis, A. Agarwal, M. Tomozawa, K. Hirao, *Quantitative infrared spectroscopic measurement of hydroxyl concentrations in silica glass*, J. Non. Cryst. Solids. **203** (1996) 27–36.

[31] C.Z. Tan, *Determination of refractive index of silica glass for infrared wavelengths by IR spectroscopy*, J. Non. Cryst. Solids. **223** (1998) 158–163.

[32] G. Navarra, I. Iliopoulos, V. Militello, S.G. Rotolo, M. Leone, *OH-related infrared absorption bands in oxide glasses*, J. Non. Cryst. Solids. **351** (2005) 1796–1800.

[33] T. Izawa, N. Shibata, A. Takeda, *Optical attenuation in pure and doped fused silica in the ir wavelength region*, Appl. Phys. Lett. **31** (1977) 33–35.

[34] H.G. Tompkins, E.A. Irene, *Handbook of Ellipsometry*, 2005.

[35] D. De Sousa Meneses, J.-F. Brun, P. Echegut, P. Simon, *Contribution of Semi-Quantum Dielectric Function Models to the Analysis of Infrared Spectra*, Appl. Spectrosc. **58** (2004) 969–974.

[36] R. Kitamura, L. Pilon, M. Jonasz, *Optical constants of silica glass from extreme*

ultraviolet to far infrared at near room temperature, Appl. Opt. **46** (2007) 8118.

[37] A.M. Efimov, V.G. Pogareva, *IR absorption spectra of vitreous silica and silicate glasses: The nature of bands in the 1300 to 5000 cm−1 region*, Chem. Geol. **229** (2006) 198–217.

[38] D. De Sousa Meneses, G. Gruener, M. Malki, P. Echegut, *Causal Voigt profile for modeling reflectivity spectra of glasses*, J. Non. Cryst. Solids. **351** (2005) 124–129.

[39] D. De Sousa Meneses, M. Malki, P. Echegut, *Structure and lattice dynamics of binary lead silicate glasses investigated by infrared spectroscopy*, J. Non. Cryst. Solids. **352** (2006) 769–776.

[40] A. Block, M. Liebel, R. Yu, M. Spector, Y. Sivan, F.J. García de Abajo, N.F. van Hulst, *Tracking ultrafast hot-electron diffusion in space and time by ultrafast thermomodulation microscopy*, Sci. Adv. **5** (2019).

[41] J.A. Nelder, R. Mead, *A Simplex Method for Function Minimization*, Comput. J. **7** (1965) 308–313.